ADVANCED OPTICAL MATERIALS
www.advopticalmat.de

Broadband and High-Sensitivity Time-Resolved THz System Using Grating-Assisted Tilted-Pulse-Front Phase Matching

*Wei Cui, Kashif Masud Awan, Rupert Huber, Ksenia Dolgaleva, and Jean-Michel Ménard**

A broadband and sensitive time-resolved terahertz (THz) configuration relying on noncollinear optical interactions is presented. This noncollinear scheme enables a higher THz generation and detection efficiency in nonlinear crystals. The concept relies on a pair of thick (2 mm) GaP crystals with a phase grating etched on their surface to achieve phase matching between a diffracted near-infrared pulse and a THz wave propagating at normal incidence. This system is compared to a standard collinear scheme based on thin (0.2 mm) crystals and, while both systems provide access to a spectral bandwidth extending up to 6.5 THz, it is found that the noncollinear configuration improves the THz signal by more than a factor of 400 and the dynamic range of the system by 30 dB at a frequency of 3 THz.

1. Introduction

Time-resolved terahertz (THz) spectroscopy is an optical characterization technique now routinely used in the spectral range between 0.5 and 3 THz to monitor microscopic interactions and resolve key signature resonances in diverse materials such as superconductors,[1–4] semiconductors,[5,6] topological insulators,[7–10] heavy fermions,[11–13] ferroelectrics,[14,15] antiferromagnets,[16] and metal-organic compounds.[17,18] One configuration commonly used for these experiments relies on a near infrared (NIR) ultrafast source and a pair of second-order nonlinear crystals to generate and detect phase-locked THz transients.[19]

Recently, there have been considerable efforts to improve time-domain THz systems by broadening their spectral window toward the high-frequency part of the spectrum without losing sensitivity at low frequencies.[20–25] In some cases, the spectral bandwidth and duration of the pulses delivered by the NIR ultrafast source determine the highest THz frequency that can be efficiently resolved by the system. This issue can be addressed with self-phase modulation inside a nonlinear medium broadening the spectrum of these ultrashort pulses and with dispersion compensation optics recompressing the pulse in the time domain.[21,22,26] In other cases, it is the second-order nonlinear crystals used for THz generation and detection that limit the accessible THz bandwidth. However, there is only a short list of candidate crystals suited for these applications since they must possess specific linear and nonlinear optical properties, including a relatively large second-order nonlinear coefficient, a high optical damage threshold (to sustain intense NIR pumping), and a low optical absorption in both the NIR and THz regions. Furthermore, the dispersion and thickness of the crystals are additional parameters that determine the nonlinear interaction length, the coherence length, and, ultimately, the THz signal strength. Interestingly, these latter parameters can be adjusted with the experimental configuration without modifying the crystal material properties. One simple method consists in selecting a crystal thickness equal to the coherence length. This ensures a constructive nonlinear build up during the THz generation and detection processes. However, for broadband applications, this condition often involves a very thin crystal,[27,28] resulting in a low THz signal amplitude due to the short interaction length. A more versatile approach consists in implementing a noncollinear geometry where an angle is formed between the directions of propagation of the NIR and THz pulses. Not only can this scheme be used to adjust phase-matching conditions, and therefore control the accessible THz bandwidth, but it can also be carried out inside a thick crystal to enable a long and efficient nonlinear process.

W. Cui, J.-M. Ménard
Department of Physics
University of Ottawa
25 Templeton Street, Ottawa, Ontario K1N 6N5, Canada
E-mail: jean-michel.menard@uottawa.ca
K. M. Awan
Stewart Blusson
Quantum Matter Institute
2355 East Mall, Vancouver, British Columbia V6T 1Z4, Canada
R. Huber
Institute of Experimental and Applied Physics
University of Regensburg
93053 Regensburg, Germany
K. Dolgaleva
School of Electrical Engineering and Computer Science
University of Ottawa
25 Templeton Street, Ottawa, Ontario K1N 6N5, Canada

The ORCID identification number(s) for the author(s) of this article can be found under https://doi.org/10.1002/adom.202101136.

DOI: 10.1002/adom.202101136

The tilted-pulse-front THz generation technique in $LiNbO_3$ is an example of noncollinear scheme utilized to generate high-field THz pulses centered around 1 THz.[29–32] A similar concept involving a phase grating located at the surface of the generation crystal has also been proposed theoretically[33–38] and demonstrated experimentally.[39,40] This surface grating design can eliminate the imaging distortions occurring in the conventional tilted-pulse-front THz setup, thus leading to an improved THz beam quality.[33,36,39] In this configuration, the grating diffracts the normally incident NIR pulse, which then propagates in a different direction than the emitted THz pulse inside the crystal. While the nonlinear interaction is intrinsically noncollinear, the general setup can remain essentially collinear,[33,35,38,39] thus easier to align since both incoming NIR and emitted THz pulses are impinging on the front surface of the crystal at normal incidence. Recently, a similar phase grating was used on the surface of a THz detection crystal to extend the accessible spectral window and enhance the overall system's sensitivity.[41]

Here we demonstrate a time-resolved THz configuration taking advantage of surface phase gratings to achieve tilted-pulse-front phase matching in both THz generation and detection processes inside thick (2 mm) gallium phosphide (GaP) crystals. A phase grating is etched directly onto the surface of these two crystals to adjust phase-matching conditions and provide access to a spectral bandwidth extending up to 6.5 THz. Most importantly, we maximize the nonlinear interaction length inside a thick crystal leading to THz signal amplitudes >20 times larger than those recorded using a standard collinear geometry relying on a pair of thin (0.2 mm thick) unpatterned GaP crystals. This enhancement factor due to a more efficient THz generation and detection processes is around 400 in signal strength. We also collect data with a standard collinear geometry using a pair of 2 mm thick unpatterned GaP crystals. This system also exhibits a relatively strong signal but the covered spectral bandwidth is limited to the frequencies below 3 THz. The results obtained with both collinear schemes show the typical tradeoff between the THz signal amplitude and the accessible spectral bandwidth. This tradeoff is circumvented in our dual-grating configuration by shifting the optimal phase-matching conditions at higher frequencies, where phase mismatch effects are more critical at a given crystal thickness.

2. Theory

In a standard collinear THz generation (or detection) geometry governed by optical rectification (OR), the phase mismatch corresponds to

$$\Delta k = k(\omega_{\mathrm{NIR}}) - k(\omega_{\mathrm{NIR}} - \omega_{\mathrm{THz}}) - k(\omega_{\mathrm{THz}}) \tag{1}$$

where $k = |\vec{k}|$ is the magnitude of the wavevector and ω is the radial frequency corresponding to any spectral component of the incident NIR pulse (ω_{NIR}) or the generated (or detected) THz pulse (ω_{THz}). In a noncollinear geometry, the phase mismatch has been defined as[30,31,41,42]

$$\Delta k = \frac{k(\omega_{\mathrm{NIR}}) - k(\omega_{\mathrm{NIR}} - \omega_{\mathrm{THz}})}{\cos\theta} - k(\omega_{\mathrm{THz}}) \tag{2}$$

where θ is the angle formed by the direction of propagation of the diffracted NIR pulse relative to the direction of propagation of the THz pulse. The condition to achieve perfect phase matching can be expressed as[43]

$$\theta = \cos^{-1}\frac{n_g(\omega_{\mathrm{NIR}})}{n(\omega_{\mathrm{THz}})} \tag{3}$$

Therefore, the angle θ can be a control knob to adjust phase matching. We consider the configuration where the NIR pulse impinges on the grating at normal incidence. Then, the diffracted orders have a pulse front parallel to the crystal surface, which corresponds to a tilt angle γ equal to the diffraction angle $\gamma = \theta = \sin^{-1}(\lambda/n\Lambda)$, where λ is the central wavelength of the NIR pulse in vacuum, n is the refractive index of the crystal and Λ is the pitch of the grating.

3. Experiments

We use a time-domain THz configuration based on an NIR ultrafast source centered at 1035 nm and delivering 60 fs pulses at a repetition rate of 1.1 MHz. Phase-locked THz transients are generated by optical rectification of these NIR pulses in a (110)-oriented GaP crystal and then detected by electro-optical sampling inside an identical crystal.[21,22] The NIR pulse incident on the THz generation crystal has a spot size of 24.8 µm ($1/e^2$ diameter) and an energy of 0.5 µJ. The NIR gating pulse incident on the THz detection crystal has a spot size of 8.2 µm ($1/e^2$ diameter) and an energy of 291 pJ if the configuration uses a phase grating at the surface of the crystal. When an unpatterned detection crystal is used instead, the gating pulse energy is reduced to 58 pJ to ensure that all the measurements are performed with the same optical power impinging on the photodiodes. This allows us to directly compare the performances of different system configurations. A mechanical stage enables point-by-point sampling of the terahertz waveform while a lock-in amplifier with a time constant of 30 and 200 ms waiting time allows sensitive acquisition of 1000 points in about 5 min. We then use the Fourier transform of the time-domain data to obtain the THz spectrum. Our tilted-pulse-front phase-matching schemes for THz generation and detection processes (schematically represented in **Figure 1**) rely on binary gratings etched at the surface of 2 mm thick GaP crystals to diffract incident NIR pulses. In the detection scheme, the THz pulse incident on the crystal is not diffracted by the periodic surface modulation due to its longer wavelength. The grating is oriented horizontally, allowing the TE-polarized NIR pulse to keep its polarization orientation unchanged upon diffraction. This geometry allows us to directly compare results obtained with diffracted and non-diffracted NIR pulses since both configurations involve the same projection of the pulses' polarization components onto the crystal's nonlinear tensor elements. The grating pitch $\Lambda = 1.635$ µm is selected from Equation (3) to satisfy phase-matching conditions between the diffracted NIR pulse and the THz component at 4 THz propagating along the

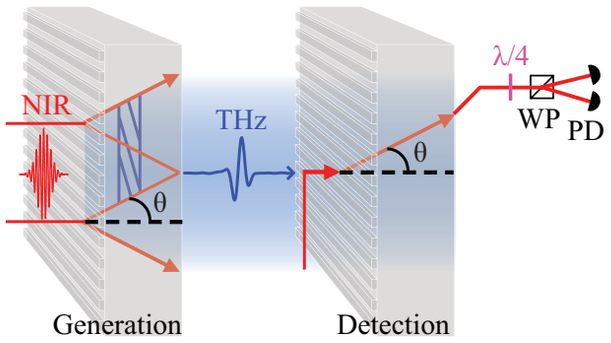

Figure 1. Schematic representation of the noncollinear dual grating configuration. A periodic modulation (Λ = 1.635 µm) at the surface of both THz generation and detection crystals diffracts the incoming NIR pulse. Tilted-pulse-front phase matching is satisfied at the frequency 4 THz. In the generation process, both first diffraction orders (m = –1, +1) contribute to the generated THz wave, while the detection relies on a single diffracted order, which is monitored in polarization as we perform electro-optical sampling. NIR: near infrared; THz: terahertz; $\lambda/4$: quarter-wave plate; WP: Wollaston prism; PD: photodetector.

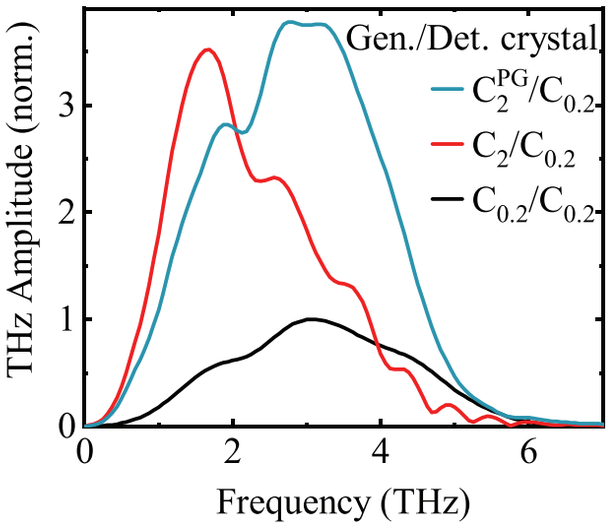

Figure 2. THz spectral amplitude measured with three different THz generation GaP crystals: $C_{0.2}$ and C_2 are unpatterned and have thicknesses of 0.2 and 2 mm, respectively, while C_2^{PG} is 2 mm thick and has a phase grating (PG) on its incident surface. Nonlinear THz detection is performed inside another $C_{0.2}$. The displayed THz spectral amplitudes are normalized by the maximum signal obtained when $C_{0.2}$ is used for both THz generation and detection processes.

direction of normal incidence, leading to a diffraction angle of 11.7° inside the GaP crystal. The grating's filling ratio is 50%, and the modulation depth is optimized to approach 245 nm during the fabrication process, which is based on the reactive ion etching (see details in Supporting Information).[41] This precise height corresponds to an optical phase difference of π to achieve destructive interference in the 0th order and maximize the signal (theoretically ≈80%) in the first diffracted orders.[44] In our experiment, we confirm a low percentage (7%) of the total transmitted power in the 0th order and obtain 61% of the transmitted power in the ±1 orders. This efficient power redistribution is crucial for efficient noncollinear THz generation involving OR of the first diffracted orders. For the noncollinear detection scheme, optimal grating diffraction in the first order is preferable, but not essential, since the detected signal is normalized by the intensity of the diffracted NIR pulse.

4. Results and Discussion

We first investigate the THz generation process with two crystals of different thicknesses and, more importantly, compare results obtained with the collinear and noncollinear geometries. As such, we measure THz signals produced inside three different generation GaP crystals with the following characteristics: 0.2 mm thick and unpatterned surface ($C_{0.2}$), 2 mm thick and unpatterned surface (C_2), and 2 mm thick with a phase grating on the incident surface (C_2^{PG}). Nonlinear THz detection is performed in this first set of experiments with another $C_{0.2}$ crystal. The black and red lines in **Figure 2** correspond to the two unpatterned generation crystals with the thicknesses of 0.2 mm ($C_{0.2}$) and 2 mm (C_2), respectively. The thickest crystal (red curve) yields the largest signal amplitude in the low-frequency part of the spectrum, while the thin crystal (black curve) possesses a larger spectral bandwidth, even leading to higher signal amplitudes at frequencies above 4 THz. These results illustrate the tradeoff between signal amplitude and spectral bandwidth. The noncollinear THz generation geometry (cyan curve) is implemented by a phase grating on a 2 mm thick crystal (C_2^{PG}) with a pitch selected to satisfy phase-matching conditions at 4 THz. This optimization of phase-matching conditions combined with the fact that low THz frequencies are inherently associated with longer nonlinear coherence lengths [45] effectively broadens the signal spectral bandwidth. In comparison with the results obtained with $C_{0.2}$, we find that the noncollinear geometry leads to a large THz spectral bandwidth and a larger signal amplitude, by a factor of 3.8 at 3 THz. The maximum amplitude obtained with C_2^{PG} is comparable to the one obtained with C_2, but it is now centered at 3 THz instead of 1.7 THz.

In another series of experiments involving the same three crystals presented above, we change the detection crystal in the electro-optical sampling part of the time-domain THz setup, while keeping $C_{0.2}$ as the generation crystal. Results in **Figure 3** obtained with the detection crystals $C_{0.2}$ (black curve) and C_2(orange curve) show a strong signal dependence on the crystal thickness, which is similar to the one seen in Figure 2 when the positions of the generation and detection crystals were inverted. In a grating-assisted noncollinear THz detection geometry, provided by C_2^{PG} (blue curve), we observe a relatively large spectral bandwidth comparable to the one obtained with $C_{0.2}$. More importantly, the relative signal amplitude is now much larger. At the peak amplitude, the signal is a factor of ≈9 higher than the one measured with $C_{0.2}$, and also a factor of ≈2 higher than the one measured with C_2. This increase is due to an intrinsic polarization filtering effect occurring at the back surface of the detection crystal.[41,46,47] Briefly, partial reflection of the s-polarized component of the diffracted NIR pulse reduces the total power on the photodiodes, while the p-polarized component containing the THz information, is preferentially transmitted. Since the THz signal is normalized

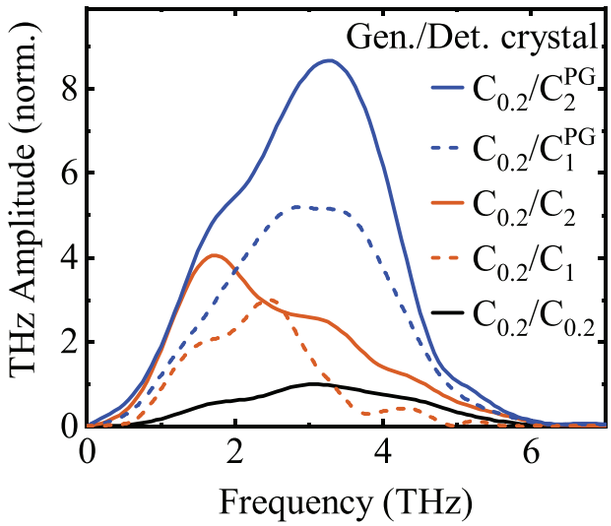

Figure 3. THz spectral amplitude measured with three different THz detection GaP crystals: $C_{0.2}$, C_1,[41] and C_2 are unpatterned and have thicknesses of 0.2, 1, and 2 mm, respectively, while C_1^{PG}[41] and C_2^{PG} are 1 and 2 mm thick, respectively, and have a phase grating (PG) on their incident surface. Nonlinear THz generation is performed inside another $C_{0.2}$ crystal. The displayed THz spectral amplitudes are normalized by the maximum signal obtained when $C_{0.2}$ is used for both THz generation and detection processes.

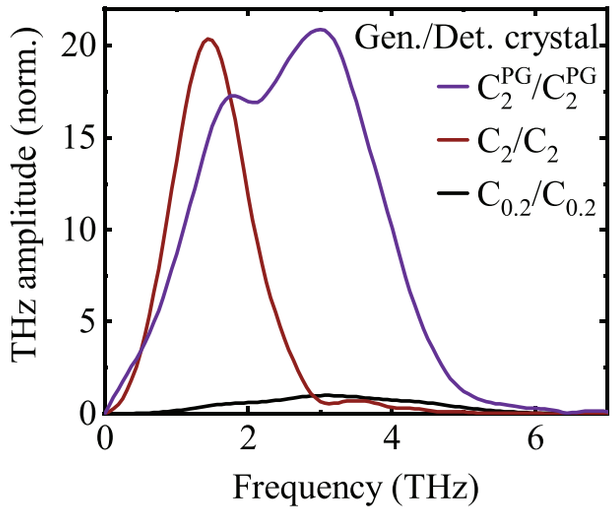

Figure 4. THz spectral amplitude measured with three pairs of identical generation and detection GaP crystals having thicknesses of 0.2 and 2 mm. A phase grating (PG) on the incident surface of a 2 mm thick crystal modulates phase-matching conditions to enhance THz generation and detection above 2 THz.

by the power incident on the photodiodes, the spectral amplitude obtained with C_2^{PG} is therefore larger. Our group also previously reported a noncollinear geometry inside a 1 mm thick GaP crystal, the results of which are added to Figure 3 for comparison (dashed lines).[41] We observe that increasing the thickness of the crystal by a factor of 2 in a noncollinear geometry increases the amplitude by a factor of 1.5. This discrepancy can be attributed to a gradual loss of spatial overlap between the NIR and THz pulses as they propagate in different directions inside the crystal. This ultimately sets a limit on the maximum angular deflection and effective crystal thickness for this detection scheme.

In a third experiment, we perform noncollinear THz generation and detection with a pair of C_2^{PG} (purple curve) and compare the measured signal amplitude with the one obtained with a pair of unpatterned $C_{0.2}$ (black curve; same shown in Figures 2 and 3) and a pair of unpatterned C_2 (dark red curve). The collinear C_2/C_2 configuration for nonlinear THz generation/detection yields a limited spectral bandwidth but a large signal amplitude peaking at 1.5 THz. This amplitude is a factor of 20 larger than the maximum spectral amplitude measured with a configuration using a pair of $C_{0.2}$. The dual patterned crystal configuration C_2^{PG}/C_2^{PG} enables a long nonlinear interaction length which contributes to a large THz peak amplitude, comparable to the one obtained with C_2/C_2, while the spectral bandwidth still extends up to 6.5 THz on a linear scale. We also perform simulations solving the coupled wave equations[45] in the frequency domain and found good qualitative agreement with our experimental data. These simulated spectra are presented in Figures S1–S4 (Supporting Information).

Figure 4 clearly indicates a net advantage in terms of signal amplitude and spectral bandwidth in using a dual noncollinear configuration in time-resolved THz spectroscopy. For any spectroscopy applications, another crucial parameter is the dynamic range allowing us to determine the ability of a system to characterize samples, especially when they are strongly absorptive. To investigate this value, we collect the THz amplitude $E(\omega)$ and the noise floor $\varepsilon(\omega)$ corresponding to the absolute square of the recorded signal when the THz pulse is blocked. The dynamic range (DR) is then defined by[48,49]

$$\mathrm{DR} = \left|E(\omega)\right|^2 / \varepsilon(\omega) \tag{4}$$

We focus on the two configurations in Figure 4 providing the largest spectral bandwidth: $C_{0.2}/C_{0.2}$ and C_2^{PG}/C_2^{PG}. **Figure 5**a shows on a log scale that both configurations yield similar spectral bandwidth, with a signal extending up to 6.5 THz, after which the spectral power approaches the noise level corresponding to the fluctuations in the THz signal amplitude. The noise floor (thinner lines in Figure 5a) is obtained by performing a regular time-resolved scan while blocking the THz beam. The noise is fitted with the model: $A^*(1/f + B)$, where both A and B are fitting parameters and f is the frequency. This model includes a term inversely proportional to the frequency to account for the flicker noise ($1/f$ noise or pink noise).[49,50] Using the fitted noise curves and spectral power curve, we extract the DR, which has a maximum of 60 dB with the $C_{0.2}/C_{0.2}$ configuration, and 90 dB with the C_2^{PG}/C_2^{PG} configuration. This 30 dB improvement is mainly due to the higher-amplitude signal generated and detected in a thick nonlinear crystal, but also partially due to the intrinsic polarization filtering effect at the back surface of the detection crystal enhancing the detection sensitivity. Overall, the dynamic range obtained with the dual grating configuration is >80 dB over a relatively broad bandwidth extending from 1.1 to 4.3 THz.

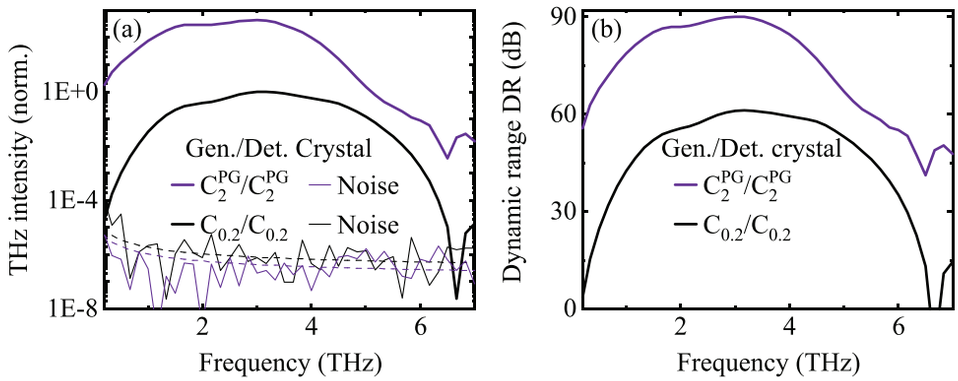

Figure 5. a) THz spectral intensities and the noise floors measured with 2 pairs of identical generation and detection GaP crystals having a thickness of 0.2 and 2 mm. A phase grating (PG) on the incident surface of a 2 mm thick crystal modulates phase-matching conditions to enhance THz generation and detection above 2 THz. The dashed lines are the noise floors fitted with the model $A^*(1/f + B)$, where both A and B are fitting parameters and f is the frequency. b) Dynamic ranges calculated based on Equation (4) and the measurement results in (a).

5. Conclusion

Our configuration based on a pair of nonlinear GaP crystals with a surface phase grating overcomes some limits imposed by phase-matching conditions at normal incidence, while allowing a longer nonlinear interaction length to achieve high signal amplitude over a large bandwidth. We notably achieve a dynamic range above 80 dB between 1.1 and 4.3 THz and obtain a peak dynamic range of 90 dB at 3 THz. This represents a 30 dB improvement in comparison to signals collected with the same system using thin (0.2 mm) unpatterned GaP generation and detection crystals.

Our system sensitivity could be further improved by combining our technique with other techniques, including a continuous data acquisition technique.[51,52] Our concept can be easily implemented in a standard THz-TDS system, since the crystals with an etched phase grating can simply replace the conventional (unpatterned) generation and detection crystals. Only minimum adjustments are required in the detection stage to direct one of the first diffracted orders into the EO detection system.

Although this work focuses only on improving spectroscopy applications in the region between 3 and 6.5 THz using GaP as a nonlinear crystal, the idea can be applied to other materials to improve THz generation and detection in other spectral regions. This technique can be applied to a wide range of nonlinear crystals and with different types of optical sources to optimize phase-matching conditions at specific THz frequencies. Table S1 (Supporting Information) shows calculated diffraction angles to achieve tilted-pulse-front phase matching in common nonlinear THz crystals for optimal THz generation and detection at 1 and 3 THz. Since our simple noncollinear geometry allows phase-matching conditions to be adjusted, a broader range of nonlinear materials may also become appealing to THz applications.[53] Finally, our results pave the way toward efficient THz spectroscopy across a broad bandwidth and could enable high-field THz generation at frequencies above 3 THz.

Supporting Information

Supporting Information is available from the Wiley Online Library or from the author.

Acknowledgements

J.-M.M. acknowledges funding from the Natural Sciences and Engineering Research Council of Canada (NSERC) Discovery Grant RGPIN-2016-04797, the Canada Foundation for Innovation (CFI) (Project Number 35269), and the Alexander von Humboldt Foundation. K.D. acknowledges Canada Research Chairs program and NSERC Discovery Grant RGPIN-2020-03989.

Conflict of Interest

The authors declare no conflict of interest.

Data Availability Statement

Research data are not shared.

Keywords

broadband, grating-assisted tilted-pulse-front phase matching, high-sensitivity, time-resolved terahertz system

Received: June 6, 2021
Revised: September 18, 2021
Published online: October 19, 2021

[1] S. Rajasekaran, J. Okamoto, L. Mathey, M. Fechner, V. Thampy, G. D. Gu, A. Cavalleri, *Science* **2018**, *359*, 575.
[2] X. Yang, L. Luo, M. Mootz, A. Patz, S. L. Bud'ko, P. C. Canfield, I. E. Perakis, J. Wang, *Phys. Rev. Lett.* **2018**, *121*, 267001.
[3] P. Chauhan, F. Mahmood, D. Yue, P.-C. Xu, X. Jin, N. P. Armitage, *Phys. Rev. Lett.* **2019**, *122*, 017002.
[4] F. Mahmood, X. He, I. Božović, N. P. Armitage, *Phys. Rev. Lett.* **2019**, *122*, 027003.
[5] E. Cinquanta, D. Meggiolaro, S. G. Motti, M. Gandini, M. J. P. Alcocer, Q. A. Akkerman, C. Vozzi, L. Manna, F. De Angelis, A. Petrozza, S. Stagira, *Phys. Rev. Lett.* **2019**, *122*, 166601.
[6] X. Li, K. Yoshioka, Q. Zhang, N. M. Peraca, F. Katsutani, W. Gao, G. T. Noe II, J. D. Watson, M. J. Manfra, I. Katayama, J. Takeda, J. Kono, *Phys. Rev. Lett.* **2020**, *125*, 167401.

[7] K. N. Okada, Y. Takahashi, M. Mogi, R. Yoshimi, A. Tsukazaki, K. S. Takahashi, N. Ogawa, M. Kawasaki, Y. Tokura, *Nat. Commun.* **2016**, *7*, 12245.
[8] J. Reimann, S. Schlauderer, C. P. Schmid, F. Langer, S. Baierl, K. A. Kokh, O. E. Tereshchenko, A. Kimura, C. Lange, J. Güdde, U. Höfer, R. Huber, *Nature* **2018**, *562*, 396.
[9] L. Luo, X. Yang, X. Liu, Z. Liu, C. Vaswani, D. Cheng, M. Mootz, X. Zhao, Y. Yao, C.-Z. Wang, K.-M. Ho, I. E. Perakis, M. Dobrowolska, J. K. Furdyna, J. Wang, *Nat. Commun.* **2019**, *10*, 607.
[10] S. Sim, S. Lee, J. Moon, C. In, J. Lee, M. Noh, J. Kim, W. Jang, S. Cha, S. Y. Seo, S. Oh, D. Kim, A. Soon, M.-H. Jo, H. Choi, *ACS Photonics* **2020**, *7*, 759.
[11] C. Wetli, S. Pal, J. Kroha, K. Kliemt, C. Krellner, O. Stockert, H. v. Löhneysen, M. Fiebig, *Nat. Phys.* **2018**, *14*, 1103.
[12] S. Pal, C. Wetli, F. Zamani, O. Stockert, H. v. Löhneysen, M. Fiebig, J. Kroha, *Phys. Rev. Lett.* **2019**, *122*, 096401.
[13] L. Prochaska, X. Li, D. C. MacFarland, A. M. Andrews, M. Bonta, E. F. Bianco, S. Yazdi, W. Schrenk, H. Detz, A. Limbeck, Q. Si, E. Ringe, G. Strasser, J. Kono, S. Paschen, *Science* **2020**, *367*, 285.
[14] S. Pal, N. Strkalj, C.-J. Yang, M. C. Weber, M. Trassin, M. Woerner, M. Fiebig, *Phys. Rev. X* **2021**, *11*, 021023.
[15] G. Folpini, K. Reimann, M. Woerner, T. Elsaesser, J. Hoja, A. Tkatchenko, *Phys. Rev. Lett.* **2017**, *119*, 097404.
[16] S. Schlauderer, C. Lange, S. Baierl, T. Ebnet, C. P. Schmid, D. C. Valovcin, A. K. Zvezdin, A. V. Kimel, R. V. Mikhaylovskiy, R. Huber, *Nature* **2019**, *569*, 383.
[17] B. Pattengale, J. Neu, S. Ostresh, G. Hu, J. A. Spies, R. Okabe, G. W. Brudvig, C. A. Schmuttenmaer, *J. Am. Chem. Soc.* **2019**, *141*, 9793.
[18] J. Nyakuchena, S. Ostresh, D. Streater, B. Pattengale, J. Neu, C. Fiankor, W. Hu, E. D. Kinigstein, J. Zhang, X. Zhang, C. A. Schmuttenmaer, J. Huang, *J. Am. Chem. Soc.* **2020**, *142*, 21050.
[19] P. U. Jepsen, D. G. Cooke, M. Koch, *Laser Photonics Rev.* **2011**, *5*, 124.
[20] K. Aoki, J. Savolainen, M. Havenith, *Appl. Phys. Lett.* **2017**, *110*, 201103.
[21] W. Cui, A. W. Schiff-Kearn, E. Zhang, N. Couture, F. Tani, D. Novoa, P. St. J. Russell, J.-M. Ménard, *APL Photonics* **2018**, *3*, 111301.
[22] A. Halpin, N. Couture, J.-M. Ménard, *Opt. Mater. Express* **2019**, *9*, 3115.
[23] J. Drs, N. Modsching, C. Paradis, C. Kränkel, V. J. Wittwer, O. Razskazovskaya, T. Südmeyer, *J. Opt. Soc. Am. B* **2019**, *36*, 3039.
[24] G. Barbiero, H. Wang, J. Brons, B.-H. Chen, V. Pervak, H. Fattahi, *J. Phys. B: At. Mol. Opt. Phys.* **2020**, *53*, 125601.
[25] D. Jang, J. H. Sung, S. K. Lee, C. Kang, K.-Y. Kim, *Opt. Lett.* **2020**, *45*, 3617.
[26] R. Piccoli, A. Rovere, Y.-G. Jeong, Y. Jia, L. Zanotto, F. Légaré, B. E. Schmidt, R. Morandotti, L. Razzari, *Opt. Express* **2019**, *27*, 32659.
[27] A. Leitenstorfer, S. Hunsche, J. Shah, M. C. Nuss, W. H. Knox, *Appl. Phys. Lett.* **1999**, *74*, 1516.
[28] R. Huber, B. A. Schmid, R. A. Kaindl, D. S. Chemla, *Phys. Status Solidi B* **2008**, *245*, 1041.
[29] J. Hebling, G. Almási, I. Kozma, J. Kuhl, *Opt. Express* **2002**, *10*, 1161.
[30] J. Hebling, A. G. Stepanov, G. Almási, B. Bartal, J. Kuhl, *Appl. Phys. B* **2004**, *78*, 593.
[31] J. Hebling, K.-L. Yeh, M. C. Hoffmann, B. Bartal, K. A. Nelson, *J. Opt. Soc. Am. B* **2008**, *25*, B6.
[32] F. Blanchard, B. E. Schmidt, X. Ropagnol, N. Thiré, T. Ozaki, R. Morandotti, D. G. Cooke, F. Légaré, *Appl. Phys. Lett.* **2014**, *105*, 241106.
[33] L. Pálfalvi, J. A. Fülöp, G. Almási, J. Hebling, *Appl. Phys. Lett.* **2008**, *92*, 171107.
[34] K. Nagashima, A. Kosuge, *Jpn. J. Appl. Phys.* **2010**, *49*, 122504.
[35] M. I. Bakunov, S. B. Bodrov, *J. Opt. Soc. Am. B* **2014**, *31*, 2549.
[36] Z. Ollmann, J. Hebling, G. Almási, *Appl. Phys. B* **2012**, *108*, 821.
[37] Z. Ollmann, J. A. Fülöp, J. Hebling, G. Almási, *Opt. Commun.* **2014**, *315*, 159.
[38] P. S. Nugraha, G. Krizsán, Gy. Polónyi, M. I. Mechler, J. Hebling, G. Tóth, J. A. Fülöp, *J. Phys. B: At. Mol. Opt. Phys.* **2018**, *51*, 094007.
[39] J. A. Fülöp, Gy. Polónyi, B. Monoszlai, G. Andriukaitis, T. Balciunas, A. Pugzlys, G. Arthur, A. Baltuska, J. Hebling, *Optica* **2016**, *3*, 1075.
[40] M. Tsubouchi, K. Nagashima, F. Yoshida, Y. Ochi, M. Maruyama, *Opt. Lett.* **2014**, *39*, 5439.
[41] A. Halpin, W. Cui, A. W. Schiff-Kearn, K. M. Awan, K. Dolgaleva, J.-M. Ménard, *Phys. Rev. Appl.* **2019**, *12*, 031003.
[42] J. A. Fülöp, L. Pálfalvi, G. Almási, J. Hebling, *Opt. Express* **2010**, *18*, 12311.
[43] A. Nahata, A. S. Weling, T. F. Heinz, *Appl. Phys. Lett.* **1996**, *69*, 2321.
[44] J. E. Harvey, R. N. Pfisterer, *Opt. Eng.* **2019**, *58*, 087105.
[45] R. W. Boyd, *Nonlinear Optics*, 4th ed., Academic Press, San Diego, CA **2020**.
[46] M. Porer, J.-M. Ménard, R. Huber, *Opt. Lett.* **2014**, *39*, 2435.
[47] S. Ahmed, J. Savolainen, P. Hamm, *Rev. Sci. Instrum.* **2014**, *85*, 013114.
[48] M. Naftaly, R. Dudley, *Opt. Lett.* **2009**, *34*, 1213.
[49] J. Neu, C. A. Schmuttenmaer, *J. Appl. Phys.* **2018**, *124*, 231101.
[50] P. Horowitz, W. Hill, *The Art of Electronics*, 3rd edition, Cambridge University Press, New York, NY, USA **2015**.
[51] B. Urbanek, M. Möller, M. Eisele, S. Baierl, D. Kaplan, C. Lange, R. Huber, *Appl. Phys. Lett.* **2016**, *108*, 121101.
[52] C. Hoberg, P. Balzerowski, M. Havenith, *AIP Adv.* **2019**, *9*, 035348.
[53] L. Tokodi, A. Buzády, J. Hebling, L. Pálfalvi, *Appl. Phys. B* **2016**, *122*, 235.